ESR study of optically enhanced phase transition in (BEDT–TTF)3Ta2F1 1

J. V. Acrivos, H. P. Hughes, and S. S. P. Parkin

Citation: The Journal of Chemical Physics **86**, 1780 (1987); doi: 10.1063/1.452178
View online: http://dx.doi.org/10.1063/1.452178
View Table of Contents: http://scitation.aip.org/content/aip/journal/jcp/86/4?ver=pdfcov
Published by the AIP Publishing

ESR study of optically enhanced phase transition in $(BEDT\text{-}TTF)_3Ta_2F_{11}$

J. V. Acrivos[a] and H. P. Hughes[b]
San Jose State University, San Jose, California 95192

S. S. P. Parkin
IBM–Almaden Research Center, San Jose, California 95193

(Received 11 August 1986; accepted 16 October 1986)

We have identified an optically enhanced magnetic phase transition in the newly synthesized organic molecular charge transfer salt, $(BEDT\text{-}TTF)_3Ta_2F_{11}$ (BEDT–TTF≡bis-ethylenedithiolotetrathiafulvalene) by ESR absorption measurements in the *X* band microwave region. At room temperature, only a doublet state ESR absorption is observed, but below 30 K several triplet ESR absorptions appear. The orientation dependence of the ESR absorption under illumination at energies near the band gaps in the material (640 nm, $T = 12$ to 5 K, $H_0 < 0.34$ *T*) indicates that there are rapid spin exchange processes with times $\tau_e < 10^{-8}$ s near 7 to 5 K along certain crystallographic directions with a temperature dependence suggesting spin-lattice relaxation times which proceed via Van Vleck "direct processes." This, to our knowledge, is the first case where the magnetic properties of a charge transfer salt are altered by the interaction with photons of energy equal to the band gaps in a low dimensional solid, providing a new, interesting way to investigate these materials.

INTRODUCTION

A new salt of BEDT–TTF has been prepared electrochemically.[1(a)] This contains an anion, $Ta_2F_{11}^-$, with a unique linear fluorine bridge between two Ta atoms. The structure is shown in Fig. 1 and is described in more detail elsewhere.[1(a)] Single crystals of this material show an ESR absorption characteristic of a weakly populated doublet state at room temperature but below 30 K we find for the first time in the BEDT–TTF class of salts, ESR absorptions characteristic of triplet states. This work also shows that the ESR absorptions of this material are substantially affected by illumination in the visible region with maximum effect for frequencies near the charge transfer bands and that these changes depend on the crystal orientation in the magnetic resonance field.

EXPERIMENTAL

The ESR data were obtained in the *X*-band region ($\nu = 9.26$ GHz) using an IBM–Bruker ER200 system. The measurements are reported relative to the growth axes which we determined were nearly parallel to the crystal axes for this pseudo-orthorhombic structure ($a = 1.6683$, $b = 1.1928$, $c = 1.2550$ nm, $\mathbf{a}\hat{\mathbf{b}} = \mathbf{c}\hat{\mathbf{a}} = 90°$, $\mathbf{b}\hat{\mathbf{c}} = 90.230°$).[1(a)] The plane of the lamellar crystals is defined by **cb**, **a** is normal to the basal planes. In the absence of illumination we observe in addition to the expected doublet ESR absorption, several triplet ESR absorptions below 30 K. We have identified three triplet exciton ESR absorptions very similar to those already observed in several TCNQ salts.[2] The doublet ESR susceptibility is essentially constant from room temperature down to near 7 K, at which point the susceptibility decreases and then below 5 K it increases by an order of magnitude at 4 K as shown in Fig. 2(a). The sample was irradiated using a Chromatix, CMX-4 laser (3mJ/ns pulse at 10 Hz near 604 nm) via a 400 μm quartz optical fiber as shown in Fig. 3(a). The sample temperature was controlled with an Oxford Instruments 9000 Dewar system. Figure 3(a) shows the ESR absorption spectra vs time under illumination at 7 K of the doublet and triplet states.

The ESR parameters for the different paramagnetic species identified in the single crystals are important in ascertaining the nature of the interactions which lead to the formation of localized states. These are described in detail in the Appendix.[3,4] In particular we note that the **g** tensors for all the absorptions have similar orientation dependences in $\mathbf{H}_0$, indicating that they arise from paramagnetic sites in similar environments. The fine structure **D**, and **g** tensors are reported here with respect to the lamellar growth axes (**abc**) which are nearly parallel to the crystallographic axes. In the **ab** plane at certain orientations the doublet ESR absorption at all temperatures is split into two lines of equal intensity ($i = 1,2$) in Fig. 4. Near 4.5 K the ESR absorption amplitudes of these lines are equal but as the temperature increases above 5 K, the low field ESR absorption at all orientations increases in width much more rapidly than that for the high field line, indicating that the spin dynamics which contribute to the relaxation mechanism are dependent on the external field orientation relative to the principal axes of the $\mathbf{g}_i$ tensors of the doublet states, $\mathbf{X}_i'\,\mathbf{Y}_i'\,\mathbf{Z}_i'$ [$\mathbf{X}_i'\hat{\mathbf{a}} = \pm 22°$ ($\pm 5°$), $\mathbf{X}_i'\hat{\mathbf{b}} = \pi/2 - \mathbf{X}_i'\hat{\mathbf{a}}$ and $\mathbf{Z}_i' \| \mathbf{c}$]. The maximum line widths are observed when the external field is $\mathbf{H}_0 \| \mathbf{X}_i'$.

One triplet ESR absorption **D** tensor has almost axial symmetry along $\mathbf{Z}_T$, the direction of the sulphur–sulphur π–π interactions between different BEDT–TTF molecules in a given stack. Its parameters are determined by least squares analysis in Fig. 5. The other two dipolar tensors **D′**, **D″** are not as well determined because of overlap with the strong doublet state. However within the accuracy of the measurements, their **g** tensors were found to be parallel to those of the strong doublet ESR absorption as indicated in Fig. 5. These are given by

[a] To whom all correspondence should be sent.
[b] Permanent address: Cavendish Laboratory, Cambridge, UK.

 0021-9606/87/041780-09$02.10

g eigenvalues: $|g_{X'X'}\ g_{Y'Y'}\ g_{Z'Z'}|$
$= |2.0125 \quad 2.0030 \quad 2.0023|;$

g eigenvectors: $|\mathbf{X}_i'\mathbf{Y}_i'\mathbf{Z}_i'| = |\mathbf{abc}| \cdot \begin{vmatrix} 0.93 & \pm 0.37 & \\ \mp 0.37 & 0.93 & \\ & & 1 \end{vmatrix}$

and,

D eigenvalues: $|\mathscr{X}\mathscr{Y}\mathscr{Z}|/\text{MHz} = |25.5 \quad 27.4 \quad -53.2|;|24 \quad 13 \quad -37|;|5 \quad -23 \quad 19|;$

D eigenvectors: $|\mathbf{X}_T\mathbf{Y}_T\mathbf{Z}_T| = |\mathbf{abc}| \cdot \begin{vmatrix} 0.28 & & -0.96 \\ & 1 & \\ 0.96 & & 0.28 \end{vmatrix}; \begin{vmatrix} 1 & & \\ & 0.7 & 0.7 \\ & -0.7 & 0.7 \end{vmatrix}; \begin{vmatrix} 1 & & \\ & -0.4 & 0.9 \\ & 0.9 & 0.4 \end{vmatrix}.$

The third triplet state ESR absorption is very weak and it becomes evident only after a phase transition which reduces the doublet ESR absorption amplitude by over one order of magnitude. This transition is represented by the equilibrium

$$\text{HT-P} \Leftrightarrow \text{LT-S}, \qquad (1)$$

where the high temperature phase (HT-P) is definitely paramagnetic and the low temperature phase spin state (LT-S) can be best described by an enhanced spin-lattice coupling. The linewidths are of the order of 10 G at room temperature, decreasing with temperature as shown in Fig. 6(a). This indicates that there are four distinct regions where the spin dynamic processes are different. Figure 7 shows the changes

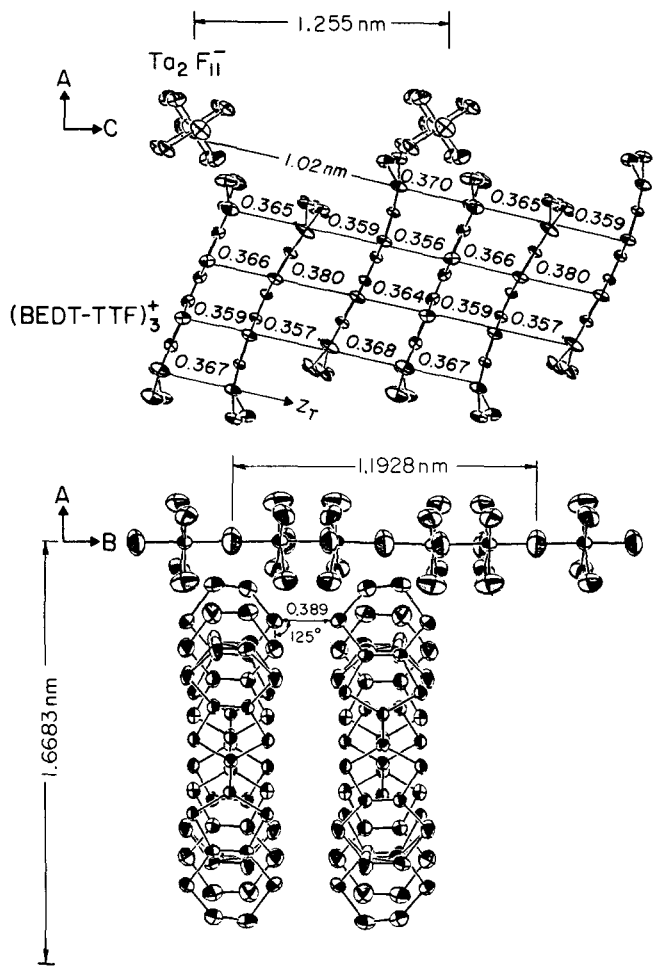

FIG. 1. Structure of $(BEDT\text{-}TTF)_3Ta_2F_{11}$ abbreviated BETa, at room temperature [Ref. 1(a)]: (a) **ac** plane structure showing sulphur–sulphur intrastack separation along the direction of the principal axis for the triplet state dipolar interaction $\mathbf{Z}_T$. (b) **ab** plane showing the closest interstack sulphur–sulphur distance along $\mathbf{Z}_T'$. The position of the protons in the ethylene groups are not determined by diffraction and are not shown here.

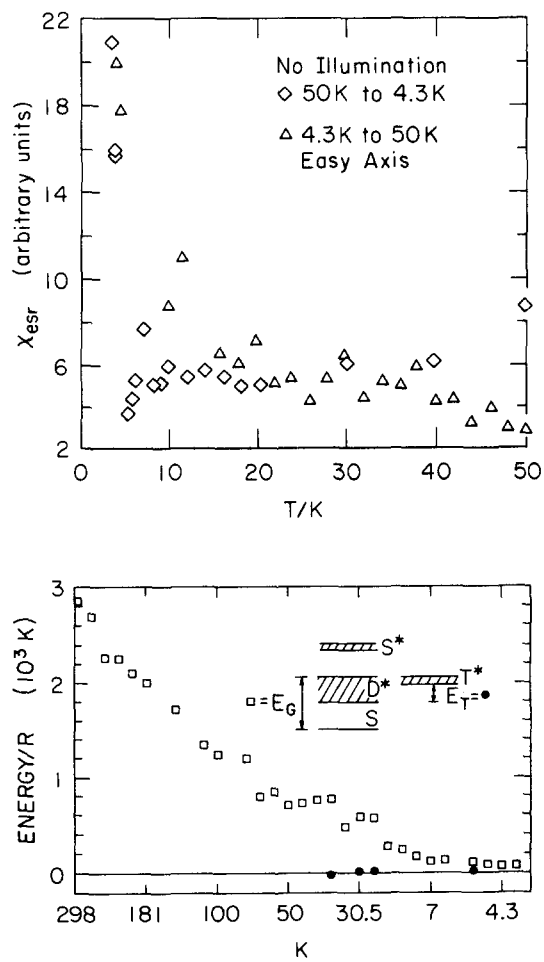

FIG. 2. ESR susceptibility vs temperature: (a) Intensities obtained under thermodynamic equilibrium without illumination. (b) Free energies E_G and E_T estimated for the chemical equilibria (2) using the intensity data and the total number N of spins 1/2 sites. Here $T\chi_{esr} \propto \Sigma_i NS_i(S_i+1)\,x_i$ where x_i is the mole fraction of the ith species, and relations (2) define $K_{2n} = \exp - E_G/RT = Nx_D^2/4(1-x_D)$ and $1/K_{2n}' = \exp E_T/RT = 3Nx_D^2/16x_T$. A free radical reference, 1,1′ bis-diphenylene, 2-phenylallyl is used in all measurements in the TE_{104} ESR cavity at room temperature as shown in Fig. 3(a).

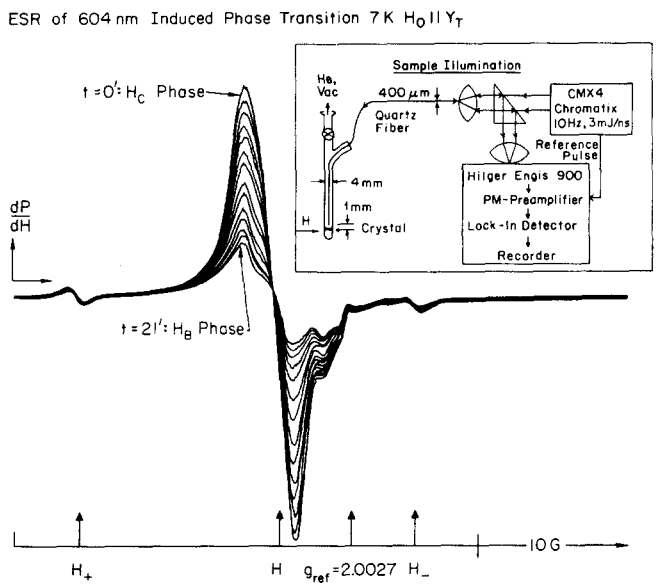

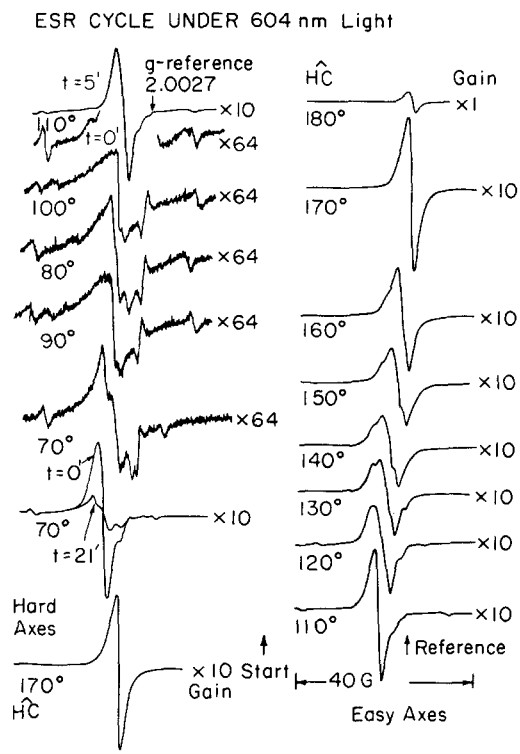

FIG. 3. ESR absorption of a single $(BEDT\text{-}TTF)_3Ta_2F_{11}$ crystal 1 $mm^2 \times 10^{-4}$ m along **a**, under pulsed illumination (3 mJ/ns pulse) with $\mathbf{H}_0$ in the **bc** plane of illumination: (a) ESR absorption vs time [each run takes 100 s and a free radical reference 1,1' bis-diphenylene, 2-phenylallyl, with $g = 2.002\,75$ (Ref. 8), is used in all measurements in the TE_{104} ESR cavity at room temperature for accurate intensity as well as field monitoring]. At $t = 0$ the crystal was rotated from $\mathbf{H}_0 \| \mathbf{c}$ to $\mathbf{H}_0 \hat{\mathbf{b}} = -20°$. The diffusion time of the excitation is estimated from the thickness of the crystal (10^{-4} m and the time it takes to reduce the doublet state signal by one half to be 10^{-7} $cm^2\,s^{-1}$. (b) Cycle of phase transitions observed by ESR absorption.

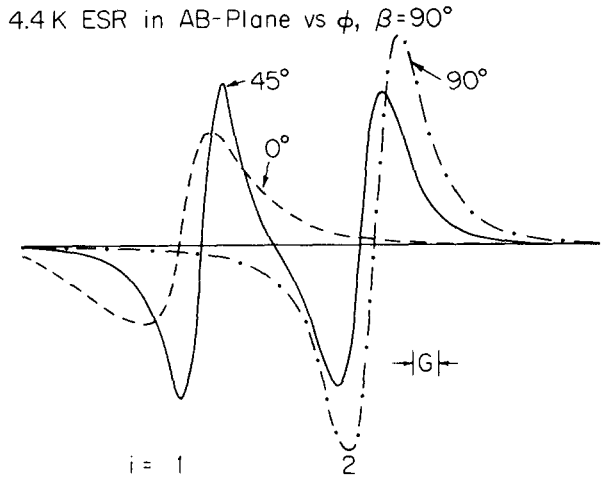

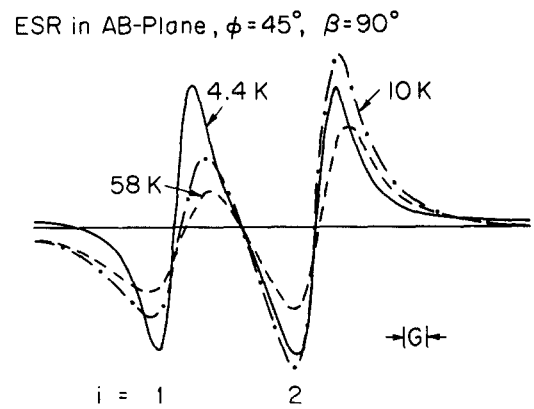

FIG. 4. ESR absorption derivature of a single crystal BETa in the **ab** plane: (a) Orientation dependence of two magnetically equivalent sites ($i = 1,2$). (b) Temperature dependence of the ESR absorption showing faster kinetic processes for the low field line.

in the ESR absorption near 5 K in the dark. These include both line broadening and resonance shifts. The spin concentration of the material was determined with a Varian TE104 dual cavity using as reference Mn^{2+}, in MgO and in aqueous solution with $\mathbf{H}_0 \| \mathbf{a}$ of a 50 μg single crystal. There are 15 to 20 molecular formula units per spin $S = 1/2$ at room temperature in this material. Since the linewidths are a qualitative measure of the temperature, they were used to estimate the effects of high photon flux on the sample temperature. The absence of line broadening by the high photon flux was then assumed to indicate that the temperature did not change appreciably. Near 5 K light emission from the sample is observed qualitatively. The absence of ^{13}C and ^{1}H hyperfine structure in the strong doublet ESR absorption suggests that the unpaired spins are either highly delocalized or that there is negligible spin density at the corresponding atoms. The latter is true for positive ion free radicals obtained by dissolving BEDT–TTF in concentrated sulphuric acid, which show no hyperfine structure and $g = 2.0060$.

DISCUSSION

The data indicates that the deviations from $g_e = 2.002\,32$ (free electron value) must arise from orbital excitations dominated by the charge distribution normal to

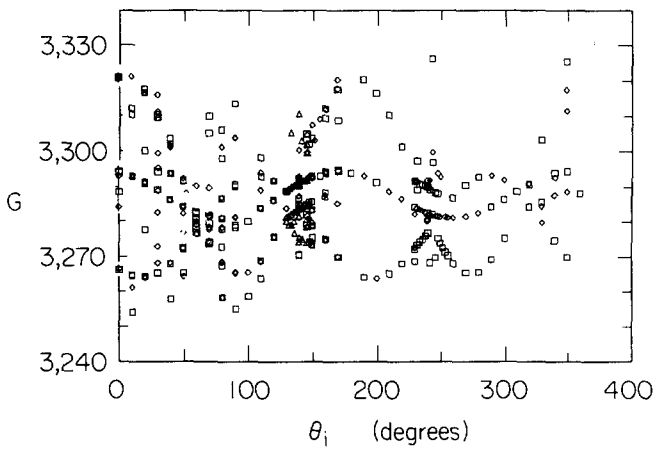

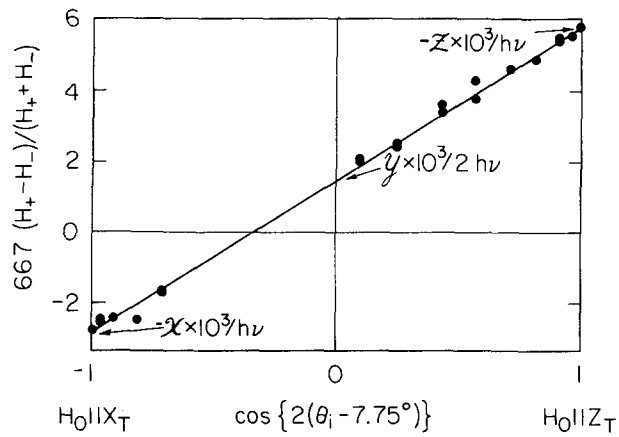

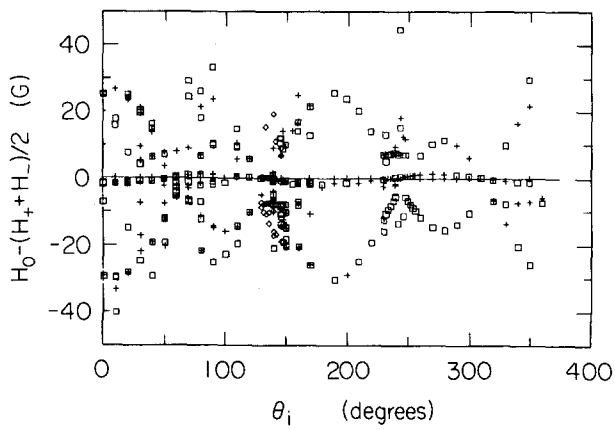

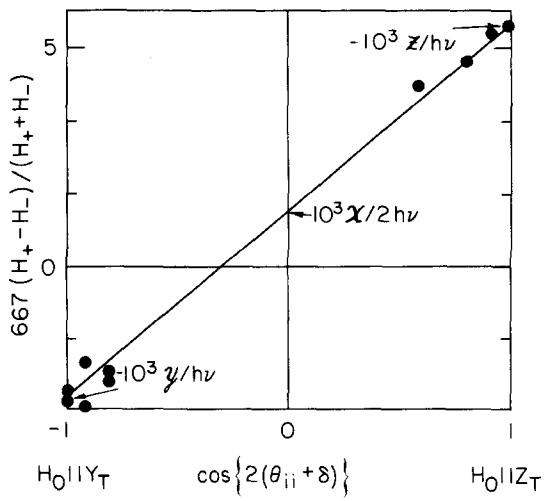

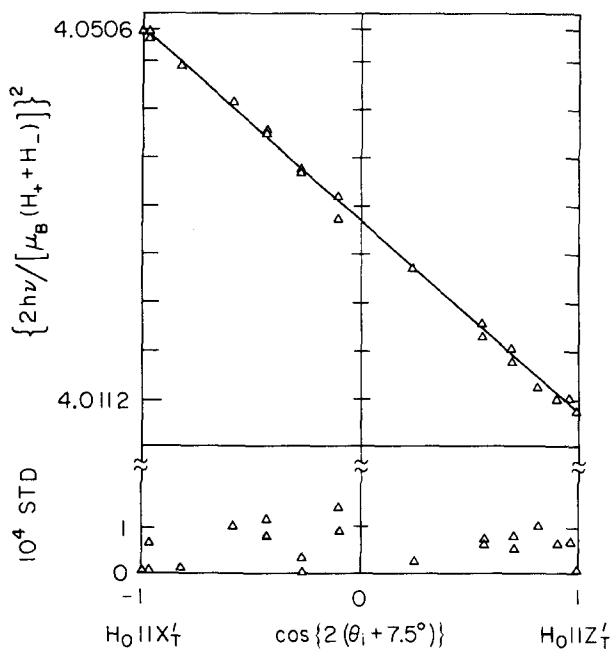

FIG. 5. Determination of the **g** and **D** tensors in the **ac** and **bc** planes of different crystals with the orientation defined in relations (A8): (a) Resonance fields for the different ESR absorptions observed near 4.5 K vs angle, $\Theta_i = \mathbf{H}_0 \hat{\mathbf{c}} - \delta$, where δ is an the alignment error defined in the Appendix. (b) Resonance fields in (a) relative to $(H_+ + H_-)/2$. (c) g_T values deduced from the data in (a). (d) Fit of the resonance fields using relations (A8) for **D** in the **ac** plane. (e) Fit of the resonance fields in using relations (A8) for **D** in the **cb** plane.

X_i' which appears to control the relaxation mechanism. The similarity of the salt's doublet ESR absorption average g tensor with that for the positive ion free radical of BEDT–TTF in concentrated sulphuric acid suggests that the former arises from isolated unpaired spins with negligible spin density near ^1H and ^{13}C. The localized monomers, say $M^{\cdot}$, must be separated by long chains of paired spins, M_{2n}, and a dynamical equilibrium between a ground singlet and excited states, represented by S, D^*, T^*, and S^*, respectively, is given by[6]

$$\begin{array}{l} \xrightarrow{k_1/4} \quad M^*_{2n+2}{:}S^* \xrightarrow{\text{decays}} M_{2n+2}{:}S \\ M_{2n+2}{:}S \overset{K_{2n}}{\Leftrightarrow} \cdot M(M_{2n})M\cdot{:}D^* \overset{k_{-1}}{\underset{}{\leftarrow}} \hat{H}(\mathbf{H}_0) \\ \xrightarrow{3k_1/4} \quad \cdot MM\cdot(M_{2n}){:}T^* \xrightarrow{\text{decays}} M_{2n+2}{:}S, \end{array} \tag{2}$$

where the equilibrium constants K_{2n}, $K'_{2n} = k_1/k_{-1}$ depend on the chain lengths (i.e., the spin–spin exchange interaction terms along the spin paired $2n$ units) and the Hamiltonian $\hat{H}(\mathbf{H}_0)$ mixes S^* and T^*. The equilibrium constants can be estimated as indicated in Fig. 2(b) and the first order rate constant for the disappearance of the doublet state k_D is estimated from the logarithmic dependence of the linewidths vs $1/T$ as indicated in Fig. 6(b). The strong doublet ESR absorption of the uncorrelated electron–hole pairs $\cdot M(M)_{2n}M\cdot$ in reaction (2) suggests that it is similar to the Chichibabin biradical polymer hydrocarbon,[7] where the ESR absorption in solution is characteristic of an isolated doublet state because of the large separation between the individual paramagnetic sites in the polymer. The room temperature susceptibility indicates that the equilibrium reaction (2) is displaced to the left, favoring the singlet state. The reaction dynamics are made evident both by the ESR linewidths and by the shifts of the resonance fields. The lifetime τ_{De} of the doublet state in reaction (2) contributes to the spin–spin relaxation time

$$1/T_{2D} = 1/T^\circ_{2D} + 1/\tau_{De}. \tag{3}$$

Here $1/T_{2D} = 3^{1/2}\,\Delta H_{MS}/2$ and ΔH_{MS} is the linewidth between the points of maximum slope of the absorption derivative for a Lorentzian shape. Figure 6 shows that the exchange rate $1/\tau_{De}$ is an activated process ($k_D \equiv 1/\tau_{De} = \Sigma_i A_i \exp - \Delta U_i/RT$) with at least four regions where the dominant terms have activation energies $\Delta U_i/R = 115$ K above 70 K, and 11 K above 11 K and, preexponential factors of $3.5*10^7\ s^{-1}$ and $0.7*10^{-5}\ s^{-1}$, respectively. Below 7 K, the activation process is more complex with $1/T_{2D}$ increasing to the room temperature value between 7 and 5 K and decreasing with temperature below 5 K at a rate which suggests that Van Vleck direct process spin lattice interactions dominate the relaxation mechanism.[3(a)] The resonance field shifts observed for the triplet excitons in Fig. 7 indicate that these are not independent of each other and that there is a dynamic equilibrium between all the paramagnetic species. The sharp triplet ESR linewidths (≈ 1 G) observed at temperatures above 7 K indicate that the rate of exchange between the magnetically inequivalent triplet excitons is in the slow limit. From the observed linewidths [Fig. 6(a)] and relation (3) it then follows that $\tau^\circ_{Te} > 2\times 10^{-8}$ s. However, there must be exchange between the three ob-

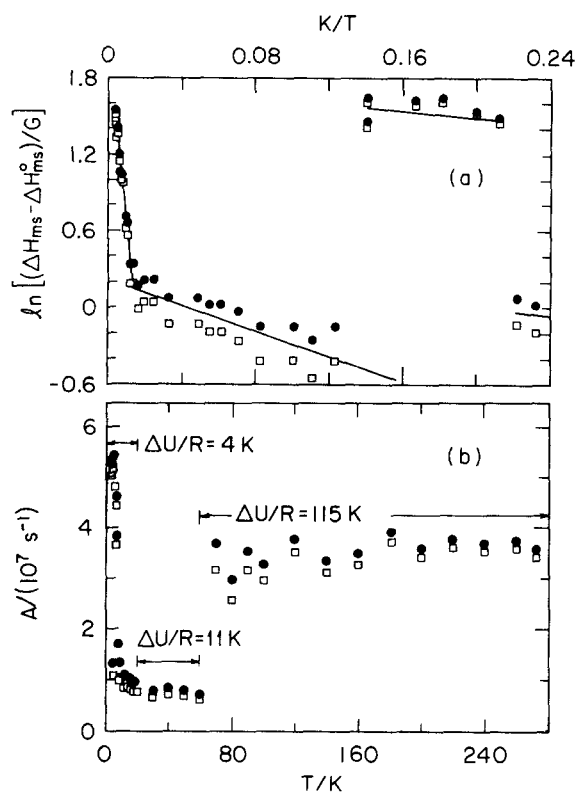

FIG. 6. Temperature dependence of the doublet ESR absorption linewidth: (a) $\ln(\Delta H_{MS} - \Delta H^\circ_{MS})$ vs $1/T$ where ΔH°_{MS} is the linewidth in the absence of chemical exchange. (b) Pre-exponential factor A for different $\Delta U/R$ values deduced from (a) and $k_D = A \exp - \Delta U/RT$. ●: $\Delta H^\circ_{MS} = 0$ and □: $\Delta H^\circ_{MS} = 0.2$ G.

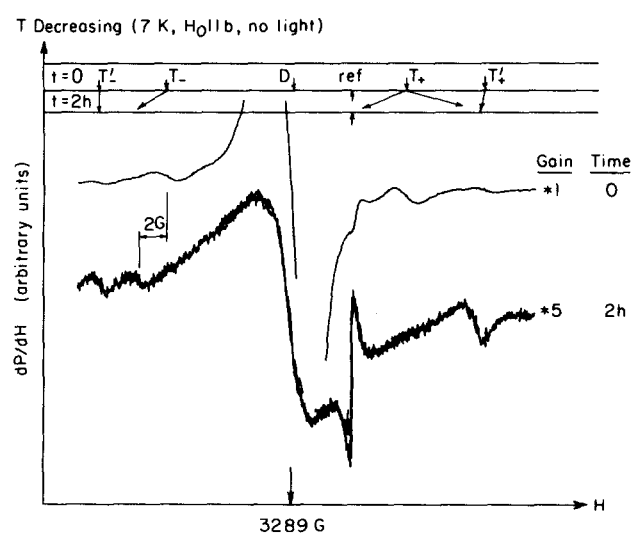

FIG. 7. ESR absorption derivative in the bc plane showing the effects of the phase transition near 6 to 7 K in the absence of illumination: (a) Before the phase transition has occurred. (b) After the phase transition has occurred. The shifts of the ESR components of two triplet excitons with fine structure tensors D and D', say T and T' indicate that this is in the intermediate rate of exchange range for the paramagnetic sites with $\tau_{Te} \approx 10^{-8}$ s [Ref. 3(b)].

served triplet excitons, the doublet and the singlet states. The phase transition observed near 7 K (Fig. 7) increases the linewidths of the D state ESR absorption and shifts the resonance fields for the components of the T states, indicating this is an intermediate exchange regime. Then according to relation (2), the exchange is governed by the rates of exchange between at least three triplet states T, T', and T'', the singlet and the doublet states. At this time all the rate constants cannot be evaluated from the scarse linewidth measurements data. $1/\tau_{Te}$, can only be estimated from the observed increased linewidths of the doublet which gives $\tau_{Te} \sim \tau_{De} < 10^{-8}$ s. This is in agreement with τ_{Te} estimated using the shifts observed in Fig. 7 between the low field components of **D** and **D'** after the phase transition and the simple textbook relation (10.31) of Ref. 3(b). However more accurate linewidth measurements are necessary to do a proper rate analysis.

The enhancement of the phase transition by the interaction with photons of energy equal to the band gaps in the material can give some information on the nature of these interactions. The parameters estimated from the fine structure tensors **D**, **D'**, **D''** will also be useful to understand these phenomena. The accurately determined dipolar tensor **D**, with nearly axial symmetry about $\mathbf{Z_T}$ in Fig. 1(a), can be interpreted using the existing theory.[3] The eigenvalues obtained from the data in Fig. 5 using relations (A8) of the Appendix, allow an estimate of the relative positions of the interacting spins **r**:

$$\mathscr{X}/h\nu = 0.5 g_{Tx}^2 \mu_B^2 \langle r^{-3} - 3x_T^2/r^5 \rangle/(h\nu) = 2.76\times 10^{-3};$$

$$\mathscr{Y}/h\nu = 0.5 g_{Ty}^2 \mu_B^2 \langle r^{-3} - 3y_T^2/r^5 \rangle/(h\nu) = 2.96\times 10^{-3};$$

$$\mathscr{Z}/h\nu = 0.5 g_{Tz}^2 \mu_B^2 \langle r^{-3} - 3z_T^2/r^5 \rangle/(h\nu) = -5.74\times 10^{-3}.$$

The signs are assigned arbitrarily in Fig. 5 because the second order terms in Eq. (A6) are less than the experimental uncertainty (1 part in 10^4). Here, $g_{Tz} = 2.0028$, $g_{Ty} = 2.0057$, $g_{Tx} = 2.0126$, and $\langle r \rangle$ is an effective separation of the center of gravity of the spin density of the interacting spins, which components (x_T, y_T, z_T) along the principal axes. The above data obtains at 9.26 GHz the expectation values in bohr^{-3} units:

$$\langle (r^2 - 3z_T^2)/r^5 \rangle = 3.03\times 10^{-4};$$

$$\langle (r^2 - 3y_T^2)/r^5 \rangle = 1.56\times 10^{-4};$$

and

$$\langle (r^2 - 3x_T^2)/r^5 \rangle = 1.44\times 10^{-4}.$$

Setting $y_T = 0$ obtains $z_T = 1.0$ nm and $x_T = 0.10$ nm or $\langle r \rangle = 1.01$ nm. This together with the fact that there is no hyperfine structure in the ESR absorption suggests that the axial fine structure tensor **D** most probably arises via the sulphur–sulphur π–π interactions along $\mathbf{Z_T}$. The spin density in the BEDT-TTF$^+$ free radical has been calculated earlier,[1(b)] but when the positive charge is distributed among three BEDT-TTF formula units, it is not possible to ascertain *a priori* the spin density in order to calculate $(\mathscr{X}, \mathscr{Y}, \mathscr{Z})$ from the room temperature crystallographic data. In Fig. 1(a) there are 12 different sulphur sites along the direction $\mathbf{Z_T}$ with alternating distances d:

Ta1.....S3– –S12– –S8 – S1 – S10– –S6– – –S5– –S9 – S2 – S7– –S11– –S4.....Ta1

d/nm = 1.03 0.37 0.37 0.36 0.36 0.37 0.38 0.37 0.36 0.36 0.37 0.37 1.02

Here the atoms are indicated by the crystallographically assigned site.[1(a)] This suggests that one cannot assign a given three BEDT-TTF formula units to a given anion, and that the spin–spin exchange interactions along $\mathbf{Z_T}$, can give rise to the singlet ground state by the antiparallel spin pairing near these sulphur–sulphur bonds. The alternating sulphur–sulphur distances indicate that the bonding is strongest near S8–S1–S10 and S9–S2–S7 above which may be due to the additional spin–spin exchange energy. The triplet ESR absorption is not observed at room temperature most probably because of fast exchange rates which lead to line broadening. Antiparallel pairing along $\mathbf{Z_T}$ only would lead to much shorter chains than is suggested by the temperature dependence of the equilibrium constant in reaction (2) as shown in Fig. 2(b). The appearance of additional triplet ESR absorptions indicates that spins can couple across the stacks, thereby increasing the chain length. The direction of the second and third triplet ESR absorption principal axes suggest that they arise from interstack spin–spin exchange interactions. The direction of closest approach, in Fig. 1(b) for sulphur atoms in the same stack is 0.356 nm and in different stacks it is 0.389 nm so that the interstack interactions would have to proceed via d orbital overlap and consequently would be weaker than the intrastack interactions. This means that the singlet chains in reaction (2) zigzag along $\mathbf{Z_T}$, $\mathbf{Z_T'}$, and $\mathbf{Z_T''}$ and the dynamic equilibrium between the different spin states proceeds via the doublet state which in turn decays to the singlet and triplet states at the rate governed by k_D given in Fig. 6(b).

The thermodynamic description is complicated. The energy separation between the ground and excited spin states follows the Lande interval rule, $W_S = JS(S+1)/2$ where $J = t^2/U$ is an effective antiferromagnetic interaction estimated in the Hubbard model,[9] for one-dimensional conductors, when t is the resonance or hopping integral between adjacent sites and U is the repulsive energy of placing two electrons (holes) in the same site. The resonance integral t varies exponentially with the distance between the overlapping orbitals (i.e., $J = J_0 \exp - d/d_0$). The population ratio near 7 K for the two triplet states in Fig. 3 gives $(J - J')/k_B = 6$ to 8 K, but J_0, d_0 remain to be determined by a Hubbard model type calculation which takes into account the lattice potential.[9(c)]

The importance of the spin–spin dipolar interactions for the phase transition near 7 K enhanced by high photon flux optical excitation with energy near U is made evident in Fig.

3(b). First we note that the equilibrium is displaced to the paramagnetic phase, with a narrow doublet ESR absorption at field orientations near $\mathbf{H_0}\|\mathbf{c}$ ($\pm 65°$). A displacement in the opposite direction, into a phase where the doublet ESR absorption amplitude is reduced due to enhanced rate processes, occurs at orientations near $\mathbf{H_0}\|\mathbf{b}$ ($\pm 25°$). This suggests that the chemical reaction induced by light excitons depends on the energy separation between the interacting paramagnetic states as was found in anthracene single crystals.[6] The reaction favors the uncorrelated electron–hole pairs at field orientations where the fine structure splitting due to $\mathbf{D}$ and $\mathbf{D}'$ is greatest (i.e., when there is no degeneracy of the ESR transitions). A displacement in the opposite direction occurs at field orientations where the splitting due to $\mathbf{D}''$ increases from nearly zero to a maximum, i.e., when there is near degeneracy between the third triplet and the strong doublet ESR absorptions, the linewidths increase indicating the increase of the rate of spin exchange when there is degeneracy between the states. In addition to the dynamic interactions between the triplet excitons, it should also be noted that populating the excited states by the transition $S \leftrightarrow S^*$, causes a change in the density of states at the Fermi level of the solid,[10] and leads to an increase in the concentration of unpaired spins by the possibility of intersystem crossing of the excited state S^* with one triplet manifold T^*, and that this will change the dynamics of reaction (2). Also the data in Fig. 7 shows that the ESR absorption intensity of the majority triplet decreases by a factor of 1.7 while that of the second triplet ESR absorption increases by a factor of 4 as a result of the phase transition. The decrease in the amplitude of the majority triplet state and the resonance field shift may be due to two possible mechanisms, an increase in linewidths due to faster relaxation times governed by relation (2) and/or to chemical reactions induced by triplet–exciton interaction as found in anthracene.[6] The increase in the ESR absorption intensity of the second triplet suggests that its concentration is enhanced by intersystem crossing, which must depend on the orientation in the magnetic field. The phase transition can be displaced in either direction of the equilibrium very slowly ($\approx$2 h) if one waits for thermodynamic equilibrium as shown in Fig. 7(b). However under illumination it can be displaced rapidly in either direction, depending on the orientation of the crystal in a moderate $\mathbf{H_0} < 0.34$ T as shown in Fig. 3(b). The coefficient for the diffusion of the excitation, starting on the illuminated surface (1 mm^2 of the crystal, at a distance of 1 mm from the optical fiber) when this is rotated from $\mathbf{H_0}\|\mathbf{c}$ at time $t = 0$ to $\mathbf{H_0} \hat{} \mathbf{b} = \pm 20°$ is estimated to be 10^{-7} cm^2/s using the time necessary for reducing the paramagnetic ESR absorption by one-half and the 0.01 mm thickness of the crystal along the **a** axis in Fig. 3(a). The paramagnetic phase is produced when the sample is illuminated at orientations about $\mathbf{H_0}\|\mathbf{c}$. A rotation about the **a** axis of the sample, with $\mathbf{H_0}$ in the **bc** plane and without illumination does not reverse equilibrium (1) in either direction in the temperature interval 5 to 12 K. But under illumination, the production of excitons reacting with the localized states associated with $M\cdot$ appears to enhance the rate of reaction. This effect, reproduced over three cycles without any changes in orientation dependence or the relative intensities, is the first observation of the enhancement of a reversible phase transition by illumination at the crystal surface and diffusion of the excitation into the bulk of low-dimensional organic conductors. It suggests that illumination can be used to vary the transport properties in a manner complimentary to pressure,[11,12] because populating the excited bands changes the density of states in the material. The most important term in reaction (2) is the exchange interaction energy term J which gives rise to a ground singlet state. The other spin states are at an energy W_S above the ground state with $2S + 1$ substates separated in energy by $h\nu$, where $k_B T > h\nu > D, D', D''$ given above. For $H_{\text{local}} \ll H_0$ the ESR absorption intensity at thermal equilibrium is given for the canonical ensemble of N spin 1/2 sites as[3,13–17]

$$I_S(T) = N(g^2\mu_B^2/3k_BT)S(S+1)\exp -(W_S/k_BT)/[\Sigma_S(2S+1)\exp -(W_S/k_BT)]\,. \quad (4)$$

The structure data suggests that there may be several ways for interstack coupling in BETa with both $W_{1/2} = E_G$ in Fig. 2(b) and $W_1 = E_G + E_T = J, J'$ or J'' being temperature dependent as already obtained for crystals of morpholinium $(TCNQ)_2$ studied recently by Oostra.[16] $W_{1/2}$ will also depend on the length of M_{2n} which keeps the uncorrelated electron–hole states isolated as in the Chichibabin polymer hydrocarbon.[7] The free energies for the reactions (2), determined in Fig. 2(c) from the ESR susceptibilities indicate a temperature dependence of J which is very similar to that for $TCNQ^-$ salts.[2,9(c),16]

CONCLUSIONS

The rapid displacement of the chemical equilibria which determine the linewidths of the ESR absorptions in BETa under illumination indicates that there is exciton interaction with the localized charge and that the magnetic field determines the direction of the reaction by producing near degeneracy of the interacting states. The alternating sulphur–sulphur distances observed within a cation stack in Fig. 1(a) (starting at a Ta atom of the $Ta_2F_{11}^-$ anion in the direction of $\mathbf{Z_T}$ going through the 12 different sulphur sites in crystal and ending at a Ta atom, 6.06 nm from the first one) indicates the existence of an alternating charge and/or spin density along the principal axis of the fine structure tensor **D**. The anisotropy of the effective $J = t^2/U$ is indicated by this work. The rapid narrowing of the ESR absorption in the range 5 to 4 K indicates that in this range, the relaxation times are long, $T_1 = T_2 > 10^{-7}$ s, and suggests a high power law temperature dependence of the relaxation time similar to that found in rare earth salts,[18] where the spin-lattice interactions are enhanced according to Van Vleck "direct-process" interactions.[3(a)] Also, the fact that the ESR linewidths scale as the components of the **g** tensor at these low temperatures suggests that the line broadening is governed by spin-phonon scattering as found in other BEDT–TTF salts.[19]

ACKNOWLEDGMENTS

This work was supported at SJSU by NSF Grant No. DMR 8303746 and we acknowledge the valuable aid in the

measurements for earlier experiments (Ref. 5), given by our associates during the time they were also supported by this grant (R. Powell, Dr. M. Coulon, Dr. A. Morrobel-Sosa, M. Chen-Lei, D. Do, and J. O. Adams) and at IBM [Ref. 1(a)] (V. Lee, S. Oostra, J. Torrance, and E. Engler). The early aid from the now defunct SF Laser Center (1985 proposals No. 1282-3) is also appreciated. We are very grateful to Dr. A. Kung and Dr. T. Ling of the SF Laser Center for valuable advice and to Professor R. W. Zare and Professor J. Brauman of Stanford University for the CMX-4 laser loan in 1986. H. P. H. wishes to thank the Cavendish Laboratory, Cambridge, UK for his sabbatical leave and the above NSF Grant for support at SJSU.

APPENDIX

The spin Hamiltonian in the absence of hyperfine structure is

$$\hat{H} = \Sigma_i \, \mu_B \mathbf{H}_0 \cdot \mathbf{g}_i \cdot \mathbf{S}_i + \Sigma'_{ij} \mathbf{S}_i \cdot \mathbf{J}_{ij} \cdot \mathbf{S}_j . \tag{A1}$$

$\mathbf{J}_{ij} = \mathbf{I}J + \mathbf{J}_a$ and the second rank tensors are given by relations (3.19) and (9.5) of Ref. 3(a); $\mathbf{g} = g_e \mathbf{I} + 2\lambda_{SO}\Lambda$; $\mathbf{S}_i \cdot \mathbf{J}_a \cdot \mathbf{S}_j = \lambda^2_{SO} \mathbf{S}_i \cdot (\Lambda_{ij} + \mathbf{D}_{ij}) \cdot \mathbf{S}_j$.

$$\mathbf{S}_i \cdot \mathbf{D}_{ij} \cdot \mathbf{S}_j = |S_{iXT} \; S_{iYT} \; S_{iZT}| \cdot \begin{vmatrix} \mathscr{X} & 0 & 0 \\ 0 & \mathscr{Y} & 0 \\ 0 & 0 & \mathscr{Z} \end{vmatrix} \cdot \begin{vmatrix} S_{jXT} \\ S_{jYT} \\ S_{jZT} \end{vmatrix} ,$$

the $\mathbf{g}$ and $\mathbf{J}_a$ tensors have principal axes, $(\mathbf{X}'\mathbf{Y}'\mathbf{Z}')$ and $(\mathbf{X}_T\mathbf{Y}_T\mathbf{Z}_T)$, respectively, $D = -1.5\,\mathscr{Z}$ and $E = -0.5(\mathscr{X} - \mathscr{Y})$ when $(\mathscr{X},\mathscr{Y},\mathscr{Z})$ are the eigenvalues of $\mathbf{D}$. $\mathbf{I}$ is the unit tensor and Λ is the angular momentum matrix which mixes the ground and excited orbital states producing the deviations of g from the free electron value g_e:

$$g_{j'j} = g_e - 2\lambda_{SO} \, \Sigma_n \langle G,L_{j'},n\rangle \langle n,L_j G\rangle / (W_n - W_G) , \tag{A2}$$

where the L_j are angular momentum operators $(j',j = X',Y',Z')$ and the sum is over excited states $|n\rangle$ with energy $W_n - W_G$ above the ground orbital state G, λ_{SO} is the spin-orbit coupling constant and here $\Lambda_{X'X'} \gg \Lambda_{Z'Z'}$, $\Lambda_{Y'Y'}$ indicates the importance of the anion layer, i.e., the crystal field effects on the mixing of the excited orbital states. The angular momentum operators transform from the molecular to the laboratory axes as[4]

$$\begin{vmatrix} 2^{-1/2}J_+ \\ J_z \\ 2^{-1/2}J_- \end{vmatrix}_{\text{lab frame}} = \mathbf{D}^1(\phi,\beta,0) \begin{vmatrix} -2^{-1/2}J_+ \\ J_Z \\ 2^{-1/2}J_- \end{vmatrix}_{\text{mol frame}} . \tag{A3}$$

(β,ϕ) are the spherical polar angles of the external magnetic field H_0 relative to the molecular axes and the transformation matrix $\mathbf{D}^1$ is given by relation (4.46) of Ref. 4.

In the molecular coordinates, with eigenstates $|S,S_Z\rangle$, (A1) is written

$$\hat{H} = \Sigma_i \, \mu_B \mathbf{S}_i \cdot \mathbf{g} \cdot \mathbf{H}_0 + D\,[S_Z^2 - S(S+1)/3] + E(S_X^2 - S_Y^2) , \tag{A4}$$

and in the laboratory coordinates, $\mathbf{H}_0 \| \mathbf{z}$, the eigenstates are $|S,S_z\rangle$ and the transformation (A3) obtains from Eq. (A4):

$$\hat{H} = \Sigma_i \, \mu_B (\mathbf{S}_i \cdot \mathbf{D}'^{1+}) \cdot (\mathbf{D}'^1 \cdot \mathbf{g}_i \cdot \mathbf{D}'^{1+}) \cdot (\mathbf{D}'^1 \cdot \mathbf{H}_0) + (\mathbf{S} \cdot \mathbf{D}^{1+}) \cdot (\mathbf{D}^1 \cdot \mathbf{D} \cdot \mathbf{D}^{1+}) \cdot (\mathbf{D}^1 \cdot \mathbf{S}) , \tag{A5}$$

and correct to second order terms in D, the $\Delta S_z = \pm 1$ transition energy is

$$h\nu = g_T \mu_B H_0 \pm [D(3\cos^2\beta - 1) + 3E\sin^2\beta\cos 2\phi\,]/2 + (D^2/8h\nu)(\sin^2 2\beta - \sin^4\beta) . \tag{A6}$$

The data give $D^2/8h\nu < 0.03$ G which is less than the accuracy of the measurements and the components of the dipolar spin–spin interaction tensors are obtained from the separation between the pair of ESR absorptions identified for the triplet state in the Zeeman region (Fig. 5). The first triplet ESR absorption, which appears near 30 K, lends itself to an accurate least squares analysis of the resonance fields vs orientation. Let $H_0 = H_+$ for the transition $|1,1\rangle \rightarrow |1,0\rangle$ and H_- for $|1,0\rangle \rightarrow |1,-1\rangle$ in Eq. (A5). Then the dipolar contributions to the transition energy are canceled in the sum of resonance fields, $H_+ + H_-$ and allows for the identification of the triplet ESR absorptions in Fig. 5(a) by the angular dependence of g_T^2 in Fig. 5(c):

$$g_T^2 = [2h\nu/(\mu_B\{H_+ + H_-\})]^2 = l'^2 g_{Tx'}^2 + m'^2 g_{Ty'}^2 + n'^2 g_{Tz'}^2 , \tag{A7}$$

where (l',m',n') are the direction cosines of the external field with respect to the principal axes $(\mathbf{X}'_T\mathbf{Y}'_T\mathbf{Z}'_T)$ of the $\mathbf{g}_T$ tensor. In the **ac** and **cb** planes the mean of the resonance fields for the triplet state coincides with that for the doublet states, as shown in Fig. 5(b) by the cancellation of the resonance field of the doublet by the mean of the strong triplet state ESR absorptions. Relations (A6) and (A7) give the resonance field ratios R for the tree principal axes orientations, i:$\mathbf{H}_0 \| \mathbf{Y}_T$, ii:$\mathbf{H}_0 \| \mathbf{X}_T$, and iii:$\mathbf{H}_0 \| \mathbf{Z}_T$ as

$$\begin{aligned} R_i &\equiv [(H_+ - H_-)/(H_+ + H_-)]_i \\ &= 0.75[(\mathscr{X} - \mathscr{Z})\cos(2\mathbf{H}_0\hat{}\mathbf{Z}_T) + \mathscr{Y}]/h\nu , \\ R_{ii} &= 0.75[(\mathscr{Y} - \mathscr{Z})\cos(2\mathbf{H}_0\hat{}\mathbf{Z}_T) + \mathscr{X}]/h\nu , \\ R_{iii} &= 0.75[(\mathscr{Y} - \mathscr{X})\cos(2\mathbf{H}_0\hat{}\mathbf{X}_T) + \mathscr{Z}]/h\nu . \end{aligned} \tag{A8}$$

$(\beta,\phi)_i = (\Theta_i + \delta, 0)$, $(\beta,\phi)_{ii} = (90°, \Theta_{ii} + \delta)$, and $(\beta,\phi)_{iii} = (90°, \Theta_{iii} + \delta)$ where the δ are tilt angles between the crystallographic axes and the triplet principal axes. They were determined by a least squares fit of the resonance field ratios (A8) vs $\cos(2[\Theta + \delta])$ in Figs. 5(d) and 5(e). The eigenvalues of the $\mathbf{D}$ tensor were obtained by a linear regression of the data to fit relations (A8) in the **ac** and **bc** planes. This was used to determine the relative tilt angles to $\pm 1°$ as well as the eigenvalues of the respective $\mathbf{D}$ tensors. For a given crystal (l',m',n') can be determined only to within an error introduced when placing the sample in the mount shown in Fig. 3(a), but the relative tilt between the principal axes of $\mathbf{g}_T$ and $\mathbf{D}$ is determined accurately using relations (A7) and (A8). In the **ac** plane the tilt is $\mathbf{Z}_T\hat{}\mathbf{Z}'_T = 16°(\pm 2°)$, and the resonance field orientation dependence for various crystals grown in different batches, as shown in Figs. 3–5 indicates that $\mathbf{Z}'_T \| \mathbf{Z}'_i \| \mathbf{c}$.

The least squares analysis of the data gives the agreement shown in Fig. 5.

[1](a) S. S. P. Parkin and J. V. Acrivos, Proceedings of the International Conference on Synthetic Metals, Japan (1986); (b) S. S. P. Parkin, E. M. Engler, R. R. Schumaker, R. Lagier, V. Y. Lee, J. Voiron, K. Carneiro, J. C. Scott, and R. L. Greene, J. Phys. (Paris) **C3**, 791 (1982); (c) S. S. P. Parkin, E. M. Engler, V. Y. Lee, and R. R. Schumaker, Mol. Cryst. Liq. Cryst. **119**, 375 (1985).

[2]J. G. Vegter, T. Hibma, and J. Kommandeur, Chem. Phys. Lett. **3**, 427 (1969).

[3](a) A. Abragam and B. Bleaney, *Electron Paramagnetic Resonance of Transition Ions* (Clarendon, Oxford, 1970), Chaps. 3 and 9; (b) J. A. Pople, W. G. Schneider, and H. J. Bernstein, *High-Resolution Nuclear Magnetic Resonance* (McGraw–Hill, New York, 1959), Chap. 10.

[4]M. E. Rose, *Elementary Theory of Angular Momentum* (Wiley, New York, 1957), relation (4.46).

[5](a) A. Morrobel-Sosa, M. Chen Lei, J. O. Adams, J. Dobrynzki, and J. V. Acrivos, Proceedings of the ACS Pacific Conference **Z3** (1985); (b) J. Adams, M. Chen Lei, A. Morrobel-Sosa, J. V. Acrivos, S. Oostra, and S. S. P. Parkin, Bull. Am. Phys. Soc. **31**, 430 (1986); (c) J. V. Acrivos, H. P. Hughes, and S. S. P. Parkin, *ibid.* **31**, 430 (1986).

[6]W. Witmer and I. Zschokke-Granacher, J. Chem. Phys. **63**, 4187 (1975); L. Altwegg and I. Zschokke-Granacher, *ibid.* **73**, 213 (1980).

[7](a) D. C. Reitz and S. I. Weissman, J. Chem. Phys. **33**, 700 (1960); (b) H. M. McConnell, *ibid.* **33**, 1868 (1960); R. K. Waring and G. J. Sloan, *ibid.* **40**, 772 (1964).

[8]J. E. Wertz, F. O. Koelsch, and J. V. Acrivos, J. Chem. Phys. **23**, 2194 (1955).

[9](a) J. Hubbard, Phys. Rev. B **17**, 494 (1978); (b) R. N. Bhatt and P. A. Lee, Phys. Rev. Lett. **48**, 344 (1982); (c) T. Hibma, Ph. D. thesis, Groningen (1974).

[10]J. V. Acrivos, *Physics and Chemistry of Materials with a Layer Structure*, edited by F. Levy (Reidel, Dordrecht, 1979), Vol. VI, pp. 33–98.

[11]D. Jerome, *Physics and Chemistry of Electrons and Ions in Condensed Matter*, edited by J. V. Acrivos, N. F. Mott, and A. D. Yoffe (Reidel, Dordrecht, 1984), p. 595.

[12]S. S. P. Parkin, *Physics and Chemistry of Electrons and Ions in Condensed Matter*, edited by J. V. Acrivos, N. F. Mott, and A. D. Yoffe (Reidel, Dordrecht, 1984), p. 655.

[13]H. Martin, *Magnetism in Solids* (London ILIFE Books, 1967), Chap. 7.

[14]S. V. Vonsovskii, *Ferromagnetic Resonance* (Pergamon, New York, 1966).

[15]Z. G. Zoos, J. Chem. Phys. **49**, 2493 (1968).

[16]S. Oostra, Ph. D. thesis, Groningen (1985).

[17](a) J. C. Bonner and M. E. Fisher, Phys. Rev. B **10**, 3217 (1964); (b) H. Shiba, *ibid.* **6**, 930 (1972).

[18]C. P. Finn, R. Orbach, and W. P. Wolf, Proc. Phys. Soc. London **77**, 261 (1961).

[19]K. Carnerio, J. C. Scott, and E. M. Engler, Solid State Commun. **50**, 477 (1984).